VDMA
Fluid Power Association

23rd ISC

International Sealing Conference

Stuttgart, Germany
Sept.30 - Oct.1, 2026

Sealing the future –
Facing the challenges of tomorrow

UNI STUTTGART

Fachverband Fluidtechnik im VDMA e. V. Lyoner Str. 18
50628 Frankfurt am Main
Germany

Phone +49 69 6603-1513
E-Mail maximilian.baxmann@vdma.eu

Internet www.vdma.eu/fluid

Influence of Chrome-Plated Rod Surface Roughness on Scratch Formation under PTFE/Bronze Band Bearing Contact in Hydraulic Cylinders

Adlan Mizan, Hans W. Caranadie

Scratch or micro-scratch on piston rod hydraulic cylinder is a problem we often see . This problem seldom taken seriously but it can cause more serious problem for example the debris of the scratched rod can lead to oil contamination , the accumulation of the debris can also lead to deeper scratch due to abrasion, film leak also more visible with the rod that has scratch. Scratch is a complex problem and had many probable cause, this paper will focus on the relationship between roughness parameter on the piston rod and scratch severity it created. The current study will use different parameter of roughness Ra, Rz,Rp and RMR on a PTFE/ 40% Bronze wear ring and will be tested up to 3.000 cycle and tested under high magnification optical microscope to see the severity of the scratch in this case the depth the scratch. The relationship then selected using Regression method to see which of the roughness parameter have more impact to the severity of the scratch and also correlation method to see if any parameter interconnected to each other.

1 Introduction

Hydraulic cylinders that come back from field service often show long scratches on the chrome-plated rod. On a single rod you can see several different shapes — deep isolated grooves, fine parallel marks, short interrupted scoring, and wide plough-like scars. This mix points to a contact that is disturbed by loose hard fragments rather than to a single steady wear mechanism. In a sealed actuator there are only a few possible sources of these fragments: dirt pulled in pass the wiper, particles already in the oil, debris worn off the guide ring, and flakes from the chrome layer itself. Hard chrome is known to contain a network of micro-cracks left over from plating [1], [2], and cyclic loading can connect chrome micro cracks and release small flakes [3].

Godet and Berthier [4], [5], [6] describe this kind of contact as a “third-body” problem: loose fragments caught between the two sliding surfaces carry part of the motion and change both friction and wear.Valleys on the rod hold fragments in place, the bearing area ratio sets the real contact pressure, and the peak-to-valley height determines how hard a trapped fragment digs into the counterface.

Our goal here is only to check if the difference roughness parameter could lead to a different scratch profile. In order to do that we isolate every third-body source we can control — oil cleanliness, ingress, bearing material, plating quality — and see what is left. We ask three questions: (i) does any pre-test roughness parameter of the chrome-plated rod predict how deep the post-test scratches will be; (ii) does the rod roughness itself change after the test, as it would if asperities were ploughing the rod; and (iii) is there anything in the post-test surface morphology that points to the chrome layer itself as a source of third-body fragments. The answers guide practical recommendations for both rod finishing and chrome plating quality control.

2 Theoretical background

2.1 Scratch formation as a third-body process

Two-body abrasive wear assumes that the harder counterface, or its asperities, plough directly into the softer body. In a guide-ring/chromed-rod contact this is implausible by design: the chrome layer (typically 800–1100 HV) is far harder than the PTFE/bronze guide ring, and the bronze fillers, although harder than PTFE, are an order of magnitude softer than the chrome [7], [8]. Direct two-body ploughing of the rod by the bearing is therefore not the expected mechanism.

Three-body abrasion offers a much better match. A small population of hard particles, intermittently entering or being generated inside the contact, becomes momentarily pinned in valleys of the rod texture or embedded in the bearing surface. While pinned, each particle ploughs a groove on the rod whose depth depends on local pressure, particle hardness and the geometric ability of the texture to retain it [4], [5]. Once the particle clears the contact, ploughing stops; a different particle, entering at a different position, produces a different scratch profile. The diverse scratch morphologies observed in field-returned rods were consistent with this picture. The distinction between the two modes is illustrated schematically in Figure 1.

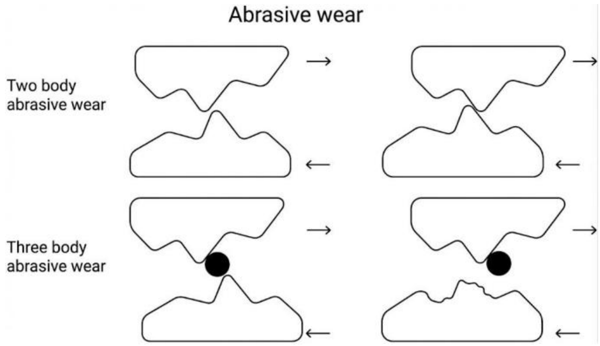

Figure 1: Two-body and three-body abrasive wear. In two-body abrasion (top), fixed asperities plough the counterface. In three-body abrasion (bottom), loose hard particles trapped in the contact produce intermittent scoring. Adapted from [9].

Each surface roughness parameter play a role with different mechanism to form a three body abrassive wear. Ra and Rz quantify the depth of available retention sites; Rp influences first contact and run-in; and the material ratio Rmr (the Abbott–Firestone bearing area ratio) governs real contact pressure [10], [11]. Higher Rmr implies more load-carrying area and distributed the load more, which should reduce scoring. These parameters co-vary in profiles produced by progressive grinding, and untangling their individual contributions is part of the experimental design in Section 3.

2.2 Possible third-body sources in a sealed hydraulic actuator

Four candidate sources of third bodies were identified before the experimental design was finalised. Oil-borne particulate contamination is bounded by the fluid cleanliness class. Atmospheric ingress is bounded by the wiper seal. Bearing-derived debris depends on the choice of guide ring material; a soft, lubricious composite such as PTFE + 40 % bronze produces a transfer film on the chrome counterface rather than hard, abrasive debris [7], [8]. The fourth candidate is the chrome layer itself: under cyclic radial load, micro-cracks in the chrome electrodeposit can propagate and release hard flakes that are then trapped in the contact [1], [2], [3]. The first three candidates can be controlled by component selection and procedure; the fourth cannot, and is the candidate most likely to remain active in a fully controlled system.

3 Experimental methodology

3.1 Specimen preparation and chrome plating

Nine identical hydraulic rod specimens were machined and hard chrome plated in the same bath, in the same parameters, to the same nominal thickness. Plating parameters are summarised in Table 1; they are reported in full so that other researchers can reproduce the chrome condition independently. The bath chemistry, current density and temperature are held within the operational window used for production rods at PT. Andalan Fluid Sistem, and a 60 s reverse etch precedes plating to promote adhesion. Post-plating, the layer hardness was measured between 60 and 63 HRC and thickness between 35 and 50 µm on all specimens, eliminating chrome quality as a deliberately varied factor.

Table 1: Hard chrome plating parameters held constant across all nine specimens.

Parameter	Value	Unit
Chromic acid (CrO_3)	250	g/L
Sulphuric acid (H_2SO_4)	3.2	g/L
Trivalent chrome (Cr^{3+})	3	g/L
Iron content	3	g/L
Catalyst	30	mL/L
Bath temperature	55–60	°C
Current density	0.45	A/cm^2
Voltage	6	V
Reverse etch	60	s
Plating time	60	min
Hardness (measured)	60–63	HRC
Thickness (measured)	35–50	µm

3.2 Roughness variation through grit pass sequences

After plating, each rod was ground using a defined sequence of abrasive grits in order to populate a range of pre-test roughness values. The nine grit pass sequences are listed in Table 2; they were chosen to span the surface finishes typically encountered on production rods at PT. Andalan Fluid Sistem, from coarse single-grit finishes to multi-step polishing through grit 1000. The specimens are referred to throughout this paper individually as S1 to S9; no further grouping is implied by their numbering. Roughness was measured perpendicular to the polishing lay using a stylus profilometer in accordance with ISO 4287 [12], and the four parameters Ra, Rz, Rp and Rmr were extracted from each profile.

Table 2: Specimen design matrix — finishing grit pass sequences.

Specimen	Grit pass sequence
S1	60, 120
S2	60, 120, 320
S3	60, 120, 320, 600, 800
S4	60, 320, 800
S5	60, 120, 600, 1000
S6	60, 120, 320, 600, 800, 1000
S7	60 finish, 1000 (single pass)
S8	320 finish, 1000 (single pass)
S9	1000 finish only

3.3 Hydraulic test rig and operating conditions

All trials were performed on a single double-acting hydraulic cylinder fitted with the seal stack listed in Table 3. The test rig schematic and a photograph of the actual test setup are shown in Figure 2. The combination of polyurethane wiper, polyurethane rod seal, PTFE with NBR energized seal and PTFE/bronze guide ring is representative of standard heavy-duty hydraulic service and was chosen specifically because every elastomeric and polymeric component is softer than the chrome counterface, which suppresses the bearing-derived hard-debris pathway. The test fluid was a mineral hydraulic oil maintained at ISO 4406 cleanliness class 18 [16],[13], filtered before each trial. Operating conditions are summarised in Table 4.

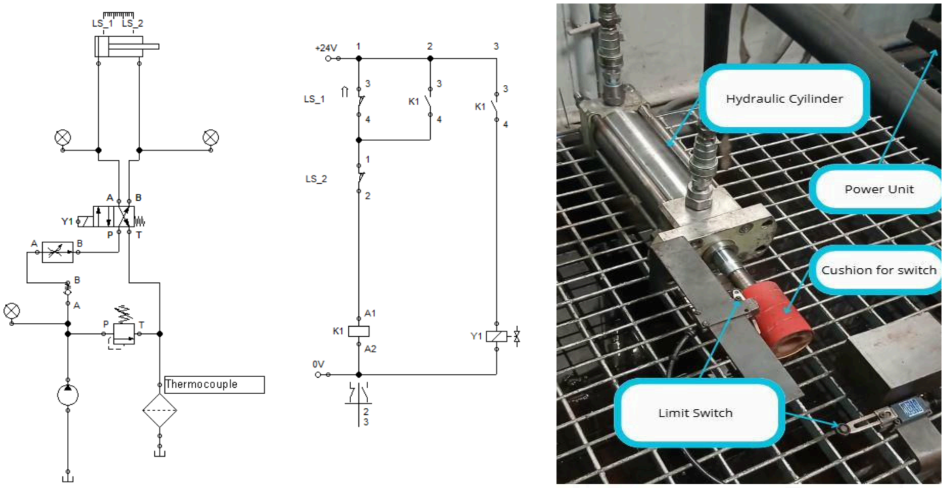

Figure 2: (a) Schematic of the double-acting hydraulic cylinder. (b) Photograph of the actual hydraulic test rig during operation.

The measurement geometry is illustrated in Figure 3. The stylus profilometer traverses perpendicular to the circumferential polishing lay to extract Ra, Rz, Rp and Rmr; the optical microscope traverses perpendicular to the longitudinal scratches to measure the deepest groove depth Rt.

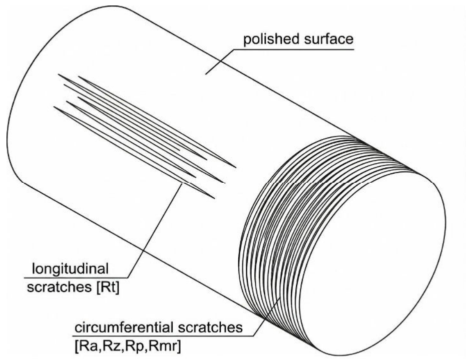

Figure 3: Measurement geometry on the chrome-plated rod. Circumferential polishing lay is characterised by Ra, Rz, Rp and Rmr; longitudinal scratches are characterised by the deepest valley depth Rt.

Figure 4 shows the assembly cross-section with the seal groove profiles; labels (a) through (c) indicate the guide ring, primary seal and wiper seal respectively.

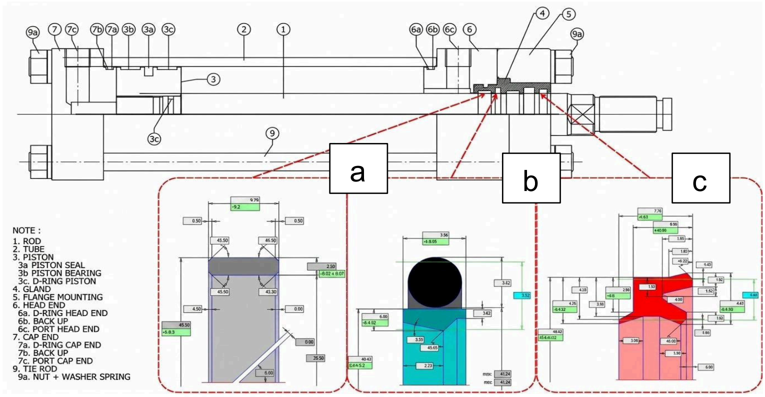

Figure 4: Assembly cross-section of the test hydraulic cylinder with expanded seal groove profiles.

The seal stack materials are listed in Table 3. The rod seal uses a U-cup polyurethane as secondary seal and a PTFE cap-seal with NBR O-ring energiser as primary seal.

Table 3: Seal stack used in all trials.

Component	Material	Type
Wiper seal	Polyurethane	DMH HPU 100
Rod seal 1	Polyurethane	DMH HPU 100
Rod seal 2	PTFE + NBR	PTFE D46
Rod guide ring	PTFE + 40 % bronze	Guarniflon G-416

Operating conditions are summarised in Table 4.

Table 4: Hydraulic test conditions.

Parameter	Value	Unit
Number of cycles	3000	–
Cycle time	3	s
System pressure	120	bar
Oil temperature range	35–60	°C
Oil cleanliness (ISO 4406)	18[16]13	–

3.4 Procedure

The procedure for each specimen proceeds as follows. (i) The rod is plated and dimensionally finished; (ii) it is ground using the grit pass sequence assigned to that specimen in Table 2; (iii) the pre-test roughness profile is measured perpendicular to the polishing lay (circumferential direction, see Figure 3) and the four parameters Ra, Rz, Rp and Rmr are recorded using stylus profilometer; (iv) the cylinder is assembled with a fresh seal stack and run for 3000 cycles at the conditions of Table 4; (v) the cylinder is disassembled, the rod is wiped clean with acetone to remove residual oil and any loose debris; (vi) the rod is examined under a high-magnification optical microscope perpendicular to the longitudinal scratch direction (see Figure 3) so that scratch profiles cross the field of view, and the deepest groove valley depth Rt of the most severe scratch found in the inspected area is recorded as the scratch severity; (vii) the rod surface is re-measured with the stylus profilometer to obtain the post-test parameters.

The deepest valley depth, denoted R_t, is taken as a single-number scratch severity descriptor and is the dependent variable for the regression analyses in Section 4.

Two forms of linear regression are employed. The single-parameter model tests each roughness parameter independently:

$$R_t = \beta_0 + \beta_1 X_i + \varepsilon \qquad (1)$$

where X_i is one of Ra, Rz, Rp or Rmr; β_0 is the intercept (the predicted scratch depth at $X_i = 0$); β_1 is the slope (the change in Rt per unit change in X_i); and ε is the residual error representing all factors not captured by the model. The general multiple-parameter model accounts for all four roughness parameters simultaneously:

$$R_t = \beta_0 + \beta_1 Ra + \beta_2 Rz + \beta_3 Rp + \beta_4 Rmr + \varepsilon \qquad (2)$$

In this form each β coefficient represents the effect of one parameter while holding the others constant. However, when predictors are strongly correlated with each other (collinear), the individual coefficients become unstable and their signs may not reflect the true physical direction of the effect [14], [15]. The degree of linear association between any two variables is quantified by the Pearson correlation coefficient r, defined as:

$$r = \Sigma[(X_i - \bar{X})(Y_i - \bar{Y})] \sqrt{[\Sigma(X_i - \bar{X})^2 \cdot \Sigma(Y_i - \bar{Y})^2]} \qquad (3)$$

Here X_i and Y_i are paired measurements and $\bar{X}$, $\bar{Y}$ are their means. The value of r lies between −1 and +1: −1 is a perfect downward straight line, +1 a perfect upward one, and 0 means no linear link at all. Its square R^2 is the share of the variation in Y that the straight-line fit on X can explain. Following Cohen [16], $|r| \geq 0.10$, 0.30 and 0.50 are read as small, medium and large effects, and Hemphill [17] notes that the median correlation in published empirical studies is about 0.21 — so values above 0.50 are already large by field-wide standards. A Pearson correlation matrix between all predictor pairs is reported alongside the regressions so that collinearity can be judged directly, and paired t-tests compare pre- and post-test roughness to check whether the trial itself shifted the surface. With nine specimens and one predictor, Equation (1) has seven residual degrees of freedom, which is enough for reliable single-parameter inference. Equation (2) is different: fitting several strongly correlated predictors on only nine specimens leaves too few degrees of freedom for the individual coefficients to be trustworthy, so the multi-parameter model is reported for its overall R^2 only and the individual β values are not read as mechanistic.

4 Results

4.1 Pre-test and post-test surface roughness

Pre-test roughness measurements for the nine specimens are summarised in Table 5. The dataset spans Ra from 0.072 to 0.423 μm, Rz from 0.677 to 3.063 μm, Rp from 0.261 to 1.137 μm, and the profile material ratio Rmr from 0.603 to 0.937 (the as-measured Rmr is reported here on the same scale as the original profilometer output and is not the post-test 0–100 % bearing-area ratio listed in Table 6). Post-test values together with the optical scratch depth Rt are listed in Table 6.

Table 5: Pre-test roughness parameters measured by stylus profilometer.

Specimen	Ra (µm)	Rz (µm)	Rp (µm)	Rmr
S1	0.423	3.015	1.137	0.634
S2	0.287	2.172	0.979	0.753
S3	0.090	0.723	0.283	0.603
S4	0.083	0.762	0.261	0.807
S5	0.085	0.745	0.293	0.779
S6	0.077	0.717	0.263	0.784
S7	0.386	3.063	0.916	0.775
S8	0.142	1.542	0.573	0.937
S9	0.072	0.677	0.309	0.928

Table 6: Post-test roughness, post-test bearing area ratio and deepest scratch depth Rt.

Specimen	Ra (µm)	Rz (µm)	Rp (µm)	Rmr (%)	Rt (µm)
S1	0.348	2.637	1.015	75.7	2.50
S2	0.124	1.128	0.351	80.8	1.00
S3	0.091	0.829	0.300	83.6	1.50
S4	0.075	0.661	0.216	80.0	1.50
S5	0.076	0.763	0.241	90.0	1.50
S6	0.074	0.600	0.213	67.2	1.40
S7	0.370	2.852	0.729	79.8	3.00
S8	0.235	1.795	0.670	70.0	1.25
S9	0.061	0.545	0.199	78.6	0.50

The pre-test roughness across all nine specimens is visualised in Figure 5. The amplitude parameters Ra, Rz and Rp vary together across the specimens, as expected from profiles produced by progressive grinding, while the bearing area ratio Rmr does not follow the same pattern. Scratch severity per specimen is plotted in Figure 6. The two largest scratch depths are observed on specimens S7 and S1, both of which have the highest pre-test amplitude roughness (Rz of 3.06 and 3.02 µm respectively). The smallest scratch depth is on S9, the smoothest specimen overall.

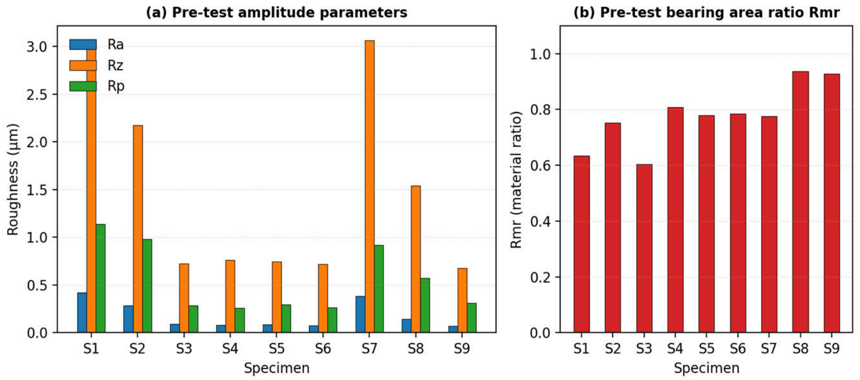

Figure 5: Pre-test roughness parameters for all nine specimens. (a) Amplitude parameters Ra, Rz and Rp. (b) Bearing area ratio Rmr.

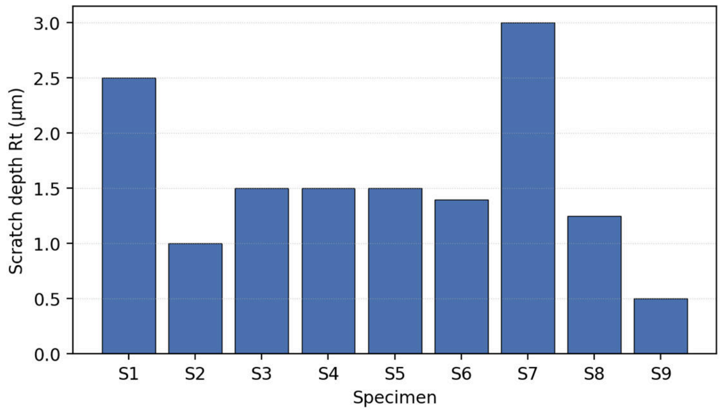

Figure 6: Deepest scratch depth Rt for each specimen.

4.2 Effect of the test on rod roughness

A natural test of two-body asperity ploughing is whether the rod gets measurably smoother after the test cycles. If the bearing is progressively flattening rod asperities, the post-test amplitude roughness should be significantly lower than the pre-test value. A paired t-test is used to evaluate this hypothesis. The test is "paired" because each specimen supplies two measurements — one before and one after the trial — and the analysis operates on the individual differences $d_i = X_{pre,i} - X_{post,i}$ rather than on raw values, thereby removing specimen-to-specimen variation in absolute roughness. The null hypothesis H_0 is that the mean difference is zero (no systematic change); the alternative H_1 is that the mean difference is non-zero (the trial has shifted the roughness). The test statistic is:

$$t = \bar{d} / (s_d / \sqrt{n}) \quad (4)$$

where $\bar{d}$ is the mean of the n paired differences, s_d is their standard deviation, and n is the number of pairs (here $n = 9$). The statistic follows a Student t-distribution with $n - 1 = 8$ degrees of freedom. If the resulting p-value exceeds the significance level $\alpha = 0.05$, the null hypothesis is not rejected and no significant change is concluded.

Figure 7 compares pre-test and post-test values of Ra, Rz and Rp side by side for all nine specimens. The visual impression is that the test reduces Ra slightly on the higher-Ra specimens and barely changes it on the smoother ones. The paired t-test results are collected in Table 8.

Table 7: Paired t-test results comparing pre-test and post-test roughness ($\alpha = 0.05$, df = 8).

Parameter	n	t-statistic	p-value	Significant?
Ra	9	0.93	0.38	No
Rz	9	1.44	0.19	No
Rp	9	1.74	0.12	No

No parameter shows a statistically significant shift at $\alpha = 0.05$ (Table 8). The highest t-value is for Rp ($t = 1.74$, $p = 0.12$), which approaches but does not cross the significance threshold. The interpretation is that the trial does not globally reshape the rod texture; whatever damage is occurring is local rather than diffuse.

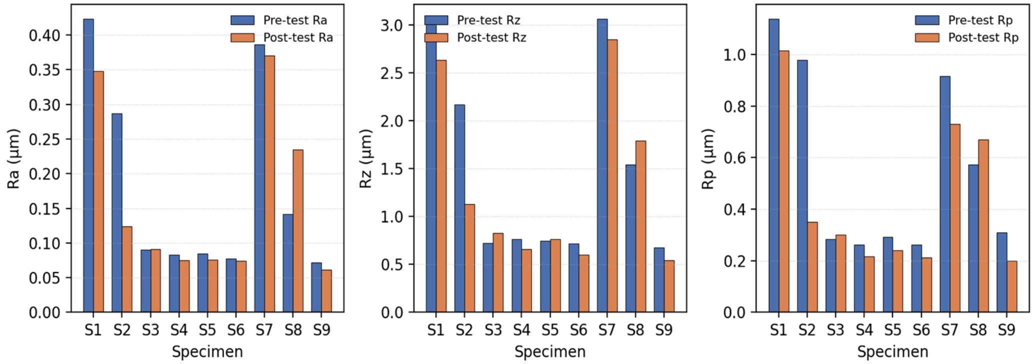

Figure 7: Pre-test versus post-test comparison of Ra, Rz and Rp for all nine specimens. No statistically significant change is observed (paired t-test p > 0.12 for all three parameters).

4.3 Regression of scratch depth on pre-test roughness

Single-parameter linear regressions of Rt on each pre-test roughness parameter are plotted in Figure 8 with regression coefficients and significance values inset. The numerical results are collected in Table 7.

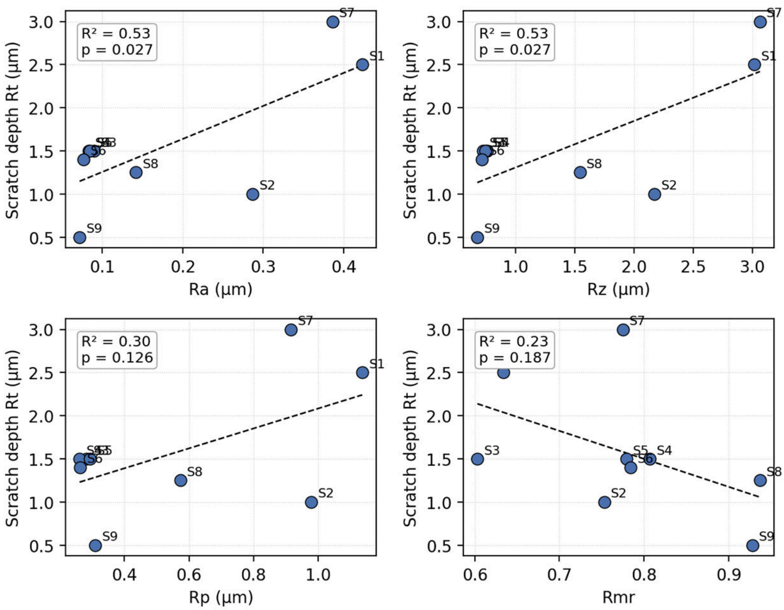

Figure 8: Linear regression of scratch depth Rt against each pre-test roughness parameter.

Table 8: Single-parameter linear regression results.

Predictor	Slope	Intercept (µm)	R^2	p-value
Ra (µm)	+3.83	+0.87	0.528	0.027
Rz (µm)	+0.54	+0.77	0.527	0.027
Rp (µm)	+1.15	+0.93	0.301	0.126
Rmr	−3.24	+4.09	0.234	0.188

Two findings stand out. First, the amplitude parameters Ra and Rz are positive and significant predictors of scratch depth at the conventional 5 % level ($p \approx 0.027$), each explaining about half of the variance in Rt. By the effect-size classification of Cohen [16], the Pearson $r \approx 0.73$ observed here falls well above the threshold for a "large" effect ($r \geq 0.50$), and Hemphill [17] reported that the median correlation in published empirical studies is $r \approx 0.21$, placing the present result in the upper range of published effect sizes. Second, the bearing area ratio Rmr enters the regression with a negative slope, in agreement with the contact-mechanics expectation that more load-carrying area implies lower local pressure and thus less aggressive scoring; however, with only nine specimens this trend does not reach statistical significance ($p = 0.19$) and must be reported as suggestive only.

The multiple-parameter model of Equation (2), fitted with the three amplitude predictors (Ra + Rz + Rp), yields $R^2 = 0.912$ and adjusted $R^2 = 0.859$ (coefficients: $\beta_0 = 1.29$, $\beta_1 = +10.65$, $\beta_2 = +0.80$, $\beta_3 = -5.14$). The overall explanatory power is considerably higher than any single predictor. However, the negative sign on β_3 (Rp) contradicts the positive univariate trend seen in Table 7 and is a classic symptom of collinearity: when near-identical predictors enter the same model, the regression distributes the shared explanatory power arbitrarily among them, producing coefficients whose individual signs and magnitudes are unreliable [14], [15]. For this reason the multi-parameter R^2 is reported as an upper bound on the total variance explained by the roughness texture, but the individual multi-parameter coefficients are not interpreted as mechanistically meaningful.

The four predictors are not independent. Figure 9 shows the Pearson correlation matrix for the pre-test roughness parameters together with Rt. Ra, Rz and Rp are nearly collinear ($|r| > 0.96$ between any pair), as expected for profiles produced by progressive grinding. This collinearity means that the regressions of Rt on Ra and on Rz are statistically interchangeable: they describe the same physical effect from two different angles, and one should not be reported as a stronger predictor than the other on the basis of these data alone.

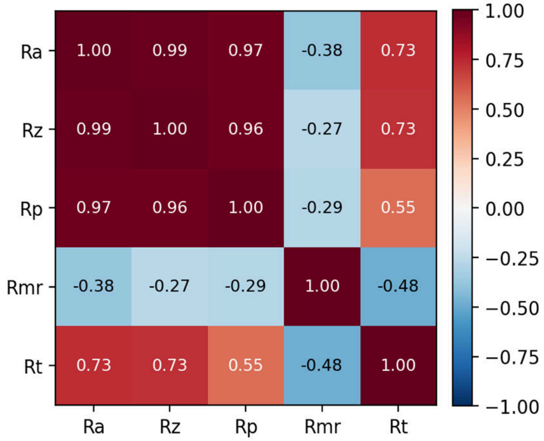

Figure 9: Pearson correlation matrix for the four pre-test roughness parameters and the scratch severity Rt.

4.4 Optical evidence of localised chrome layer defects

The optical inspection performed in step (vi) of the procedure was carried out perpendicular to the longitudinal scratch direction (see Figure 2) so that scratch profiles cross the field of view. On several specimens, including S2 shown in Figure 10, isolated micro-pits were observed within the scratched region. The profile reconstructed across one of these features gives a depth of 2.58 µm, similar in magnitude to the deepest scratch valleys recorded on the other specimens. The pit is too shallow and too localised to be a corrosion feature, and it is surrounded by parallel scoring marks running in the direction of rod travel. This morphology is consistent with a small fragment having detached from the chrome layer at this location and being subsequently dragged along the rod by the contact, ploughing the streamer pattern visible downstream.

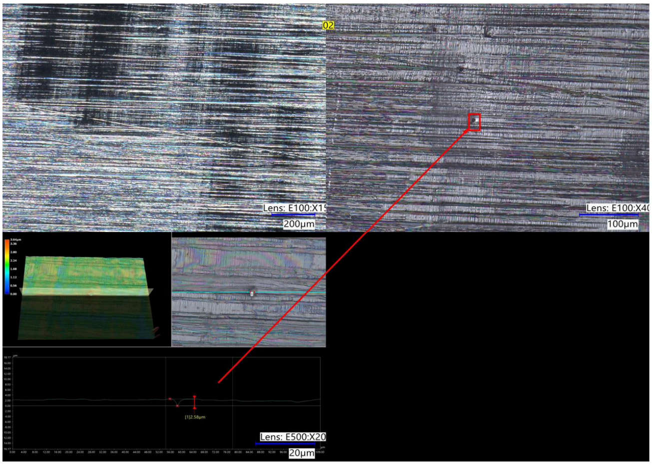

Figure 10: Optical and reconstructed profile of a localised chrome layer micro-pit on specimen S2. Top left: low-magnification view showing the polishing lay and parallel scratch streamers; top right: higher magnification of the same region; bottom left: 3D reconstruction and line profile across the pit, depth 2.58 µm.

5 Discussion

5.1 Interpretation of the correlation

The headline finding is a positive linear association between pre-test amplitude roughness and post-test scratch depth, with Pearson $r \approx +0.73$ for both Ra and Rz ($R^2 \approx 0.53$, $p \approx 0.027$, $n = 9$). Because Ra and Rz are themselves almost perfectly collinear in this dataset ($r = 0.989$, Figure 9), the two regressions should be read as a single piece of evidence shown two ways rather than as two independent confirmations. The bearing area ratio Rmr enters with the expected negative sign (Table 7) but does not reach significance at this sample size.

A significant correlation does not establish causation, and the present data are consistent with two physical readings. In the first, the texture itself is operative: deeper valleys retain trapped fragments more firmly, so any pinned third body ploughs a deeper groove. In the second, the grinding step is operative: a coarser grit sequence simultaneously leaves higher amplitude roughness and more subsurface chrome damage (residual stress, micro-crack density, nascent flake sites [1], [2], [3]), so Ra serves as a marker of finishing aggressiveness rather than as a direct cause of Rt. The two readings are not mutually exclusive and predict the same correlation, but they have different practical implications and the present dataset cannot discriminate between them.

What can be ruled out, on the other hand, is pure two-body asperity ploughing. Hard chrome at 800–1100 HV cannot be ploughed by the PTFE matrix, and the bronze fillers remain far softer than the chrome [7], [8]. The paired comparison of Section 4.2 provides direct experimental support: if rod asperities were being progressively flattened by the bearing, Ra and Rz would fall significantly between pre- and post-test measurements, and they do not ($p = 0.38$ and 0.19). The scratching process must therefore be local and intermittent rather than diffuse. Consistent with this, optical inspection of S2 revealed an isolated, shallow chrome-layer pit at the head of parallel streamers running with rod travel (Figure 10). The morphology is consistent with the release and subsequent ploughing of a small chrome fragment, offered here as a proposed contributing third-body mechanism; chemical confirmation by SEM–EDS mapping of the streamer interiors remains outstanding.

5.2 Limitations

The present investigation is a pilot study and its conclusions should be read with its limits in view. With $n = 9$ specimens the Pearson estimate is sensitive to individual points, especially S1 and S7 at the high-amplitude corner. The near-perfect collinearity of Ra, Rz and Rp (all pairwise $r > 0.96$) prevents any reliable multi-parameter regression: a combined fit achieves a high R^2 only as an artefact of the redundancy, not as a genuine discovery. The test matrix used a single oil grade, a single pressure and a single bearing material, so the observed correlation cannot yet be generalised beyond these conditions. The proposed chrome micro-flaking mechanism rests on a single profiled pit and has not been confirmed chemically. The analysis is further based on two-dimensional stylus profiles and does not capture the three-dimensional topography that may govern fragment retention [19].

Two further limitations concern the counterface and the lubricant. The PTFE + 40 % bronze guide ring was inspected only superficially; no dimensional wear measurement, no transfer film quantification and no mass-loss analysis were performed, so the wear partitioning between rod and ring remains unknown and any contribution of bronze particles to the third-body population cannot be ruled in or out. Likewise, the hydraulic oil was specified to ISO

4406 16[14]11 at the start of each trial but was not re-analysed afterwards. The gaps represent a clear direction for follow-up instrumentation.

6 Summary and Conclusion

Nine chrome-plated rod specimens, ground to different roughness levels via varying grit pass sequences, were run for 3000 cycles in a hydraulic cylinder against a PTFE + 40 % bronze guide ring at 120 bar. Within the limits of a nine-specimen pilot study, the following conclusions are supported.

The deepest scratch depth Rt correlates positively with the pre-test amplitude roughness (Pearson $r \approx 0.73$ for Ra and Rz, $R^2 \approx 0.53$, $p \approx 0.027$). Ra and Rz are nearly collinear ($r = 0.989$) and represent a single piece of evidence. Two physical readings are consistent with the data: (i) deeper valleys retain trapped fragments, causing deeper ploughing; or (ii) coarser grinding simultaneously produces higher roughness and more subsurface chrome damage, with the latter driving Rt. The present data cannot distinguish between these readings. Rmr enters with the expected negative sign but does not reach significance.

Pre- and post-test roughness do not differ significantly (paired t-test $p > 0.12$), ruling out two-body asperity ploughing and indicating that scratch formation is local and intermittent. Optical inspection reveals isolated micro-pits at the head of parallel scratch streamers, consistent with localised chrome flake release acting as in-situ third bodies.

7 Nomenclature

Variable	*Description*	*Unit*
Ra	Arithmetic mean roughness	µm
Rz	Maximum height of profile	µm
Rp	Maximum profile peak height	µm
Rt	Maximum profile valley depth (scratch severity)	µm
Rmr	Material ratio (Abbott–Firestone bearing area ratio)	– or %
p	System pressure	bar
T	Oil temperature	°C
HV	Vickers hardness	–

Variable	*Description*	*Unit*
HRC	Rockwell C hardness	–
R^2	Coefficient of determination	–
$\bar{d}$	Mean of paired differences (pre − post)	µm
s_d	Standard deviation of paired differences	µm
α	Significance level	–

8 References

[1] Pina, J., Dias, A., François, M., Lebrun, J.L.: Residual stresses and crystallographic texture in hard-chromium electroplated coatings, In: Surface and Coatings Technology, Vol. 96, pp. 148–162, 1997

[2] Suarez, O.M., Fernández, A.L., Vargas, M.: Failure analysis of chromium plating layer on the surface of the piston rod of a hydraulic jack, In: Engineering Failure Analysis, Vol. 109, 104291, 2020

[3] Wang, S., Ma, C., Walsh, F.C.: Alternative tribological coatings to electrodeposited hard chromium: a critical review, In: Transactions of the IMF, Vol. 98, No. 4, pp. 173–185, 2020

[4] Godet, M.: The third-body approach: a mechanical view of wear, In: Wear, Vol. 100, pp. 437–452, 1984

[5] Berthier, Y.: Experimental evidence for friction and wear modelling, In: Wear, Vol. 139, pp. 77–92, 1990

[6] Berthier, Y., Vincent, L., Godet, M.: Velocity accommodation sites and modes in tribology, In: European Journal of Mechanics A/Solids, Vol. 11, No. 1, pp. 35–47, 1992

[7] Trabelsi, M., Kharrat, M., Dammak, M.: Impact of lubrication on the tribological behaviour of PTFE composites for guide rings application, In: Bulletin of Materials Science, Vol. 39, pp. 1119–1127, 2016

[8] Aleksendrić, D., Ćirović, V., Smít, M.D.Á., Brătucu, G.: Tribological behaviour of hydraulic cylinder coaxial sealing systems made from PTFE and PTFE compounds, In: Polymers, Vol. 12, No. 1, 155, 2020

[9] Hasan, M.S., Kordijazi, A., Rohatgi, P.K., Nosonovsky, M.: Tribology of engineered surfaces, In: Handbook of Nanomaterials for Manufacturing Applications, Elsevier, 2023, https://doi.org/10.1016/B978-0-12-821381-0.00004-1

[10] Shabani, F., Mite, A., et al.: Mathematical modeling of the bearing ratio curve Rmr, In: Advances in Tribology, Vol. 2024, Article 5541719, 2024

[11] Greenwood, J.A., Williamson, J.B.P.: Contact of nominally flat surfaces, In: Proceedings of the Royal Society A, Vol. 295, pp. 300–319, 1966

[12] ISO 4287:1997, Geometrical product specifications (GPS) – Surface texture: Profile method – Terms, definitions and surface texture parameters, International Organization for Standardization, Geneva

[13] ISO 4406:2021, Hydraulic fluid power – Fluids – Method for coding the level of contamination by solid particles, International Organization for Standardization, Geneva

[14] Montgomery, D.C., Peck, E.A., Vining, G.G.: Introduction to Linear Regression Analysis, 5th ed., Wiley, New York, 2012, ISBN 978-0-470-54281-1

[15] Hutchings, I.M., Shipway, P.: Tribology: Friction and Wear of Engineering Materials, 2nd ed., Butterworth–Heinemann, Oxford, 2017, ISBN 978-0-08-100910–9

[16] Cohen, J.: Statistical Power Analysis for the Behavioral Sciences, 2nd ed., Lawrence Erlbaum Associates, Hillsdale, 1988, ISBN 0-8058-2283-9

[17] Hemphill, J.F.: Interpreting the magnitudes of correlation coefficients, In: American Psychologist, Vol. 58, No. 1, pp. 78–79, 2003

[18] Dobrinsky, A., Bauer, F. et al.: Advanced characterization of counter surfaces in linear applications, In: 22nd International Sealing Conference, Stuttgart, Germany, 2024, https://doi.org/10.6131/ISC22.027

[19] Engelfried, M., Baumann, M., Bauer, F.: From tactile to optical — Advancements in shaft lead analysis, In: 22nd International Sealing Conference, Stuttgart, Germany, 2024, https://doi.org/10.6131/ISC22.028

[20] International Sealing Conference (ISC), 23rd ISC Stuttgart, September 2026, https://sealing-conference.com/

9 Authors

PT. Andalan Fluid Sistem, Research and Development Division, Indonesia

Adlan Mizan, Engineer, R&D Division

Hans W. Caranadie, Engineer, R&D Division

https://doi.org/10.61319/85PWHCV9